Effects of Plasma Reactants on Atomic Layer Deposition of Lithium Phosphate and Lithium Phosphorus Oxynitride Electrolyte Films

Tohru Tsuruoka*[1], Samapika Mallik[1], Takuji Tsujita[2], Yuu Inatomi[2], and Kazuya Terabe[1]

[1]Research Center for Materials Nanoarchitectonics, National Institute for Materials Science, Tsukuba, Ibaraki 305-0044, Japan
[2]Research and Development Center, Panasonic Energy Co. Ltd, Kadoma City, Osaka 571-8501, Japan

Abstract

The effects of plasma reactants on the plasma-assisted atomic layer deposition (ALD) of lithium phosphate are investigated in relation to the fabrication of high-quality lithium phosphorus oxynitride (LiPON) thin films for the potential use as a solid-state electrolyte (SSE) in both microbatteries and neuromorphic devices. Our ALD processes enable the incorporation of nitrogen into a lithium phosphate matrix, using lithium *tert*-butoxide and tris(dimethylamino)phosphine as the lithium and phosphorus precursors, respectively, in a deposition temperature window of 220-300 °C. With O_2 plasma, polycrystalline lithium phosphate films, with a relatively well-arranged pyrophosphate, are deposited. Amorphous LiPON films, with a mixture of pyrophosphates and orthophosphate, are obtained when Ar or NH_3 plasma is used. When the NH_3 flow rate increases, the nitrogen composition increases up to ~13%, while residual carbon is kept to below a few percent. For a $Li_{2.5}PO_{1.9}N_{0.8}$ film deposited at 300 °C with NH_3 plasma, the ionic conductivity is measured as $1.65 \pm 0.42 \times 10^{-6}$ S/cm at 25 °C, with an activation energy of 0.66 eV. This conductivity is the highest value of any ALD LiPON film reported to date. Our ALD processes exhibit a high level of controllability of the molecular structures of the phosphorus oxynitride matrix, with high ionic conductivity, which makes them suitable for realizing high-performance Li SSE thin films.

1. Introduction

In the past few decades, research on lithium (Li) solid-state electrolyte (SSE) films has expanded to include a broad range of applications. In battery applications, for example, Li SSE films are used to make all-solid-state, thin-film ion batteries, which can potentially solve many problems inherent in liquid electrolyte ion batteries, such as their flammability, limited voltage, unstable electrolyte-electrode interface formation, and poor cycling performance [1] [2] [3]. Therefore, solid-state batteries are particularly attractive for safety-critical applications, such as electric vehicles, aircraft power systems, human-integrated wearable devices, and implantable electronic devices [4]. Further, increasing attraction has focused on applications for Li SSE films to electrochemical ion-insertion devices, such as electrochromic windows, thermal transistors, and electrochemical random-access memories (ECRAMs) [5]. In a typical ECRAM, the electronic conductivity of a mixed ion-electron conductor channel in a transistor (or a mixed ion-electron conductor layer in a two-terminal device) can be changed in an analog manner, based on intercalation and de-intercalation of Li ions through an SSE layer under voltage or current bias [6] [7] [8] [9] [10]. These analog switching devices are expected to be used as artificial synaptic elements in future neuromorphic computing systems, which operated with high efficiency and low-power consumption.

Lithium phosphorus oxynitride, called LiPON, is one of the most popular Li SSE materials, because of its relatively high ionic conductivity up to 10^{-6} S/cm and improved stability to the atmosphere, when compared to lithium phosphate. Various fabrication methods have been reported for LiPON films, including radio-frequency (RF) reactive sputtering [11], pulsed laser deposition [12], and metal-organic chemical vapor deposition (MOCVD) [13]. However, these techniques are not suitable for the fabrication of uniform, pinhole-free, and conformal SSE thin films onto three-dimensionally microbatteries and integrated device structures. In some methods, like MOCVD, a high deposition temperature (500 °C) is required, which in turn degrades other constituent materials or melts Li metal electrodes. Atomic layer deposition (ALD) is a promising technique for fabricating Li SSE thin films, because it can accurately deposit controlled thickness, pinhole-free, high uniformity SSE films with atomic-level precision on complex structures [14]. Kozen et al. reported plasma-assisted ALD of LiPON using lithium *tert*-butoxide (LiO^{t}Bu) and trimethylphosphate (TMP) as Li and phosphorus (P) precursors, respectively [15]. It was found that water exposure after LiOtBu helps complete the reactions, resulting in a decrease in the amount of residual carbon in the deposited films. The application of N_2 plasma after TMP allowed for the growth of LiPON with a nitrogen content of up to ~16%. Nisula et al. reported thermal ALD of LiPON using lithium hexamethyldisilazide (LiHMDS) and diethyl phosphoramidate

(DEPA) as the alternative Li and P precursors [16]. The deposited films contained ~10% nitrogen, and residual carbon of ~10% remained. Pearse et al. developed a LiOtBu - DEPA process to realize the deposition of LiPON films with a composition close to the stoichiometric Li_2PO_2N [17]. Put et al. reported the ALD of LiPON using LiO^tBu and TMP precursors with N_2 plasma [18]. They demonstrated that the ionic conductivity increased by increasing plasma power and decreasing deposition temperature. All these ALD LiPON films exhibited Li-ion conductivities of 5~6.6 × 10^{-7} S/cm at 25 °C.

In 2019, we proposed a plasma-assisted ALD process of a magnesium phosphate film using tris(ethylcyclopentadienyl)magnesium and tris(dimethylamino)phosphine (TDMAP) as the Mg and P precursors [19] [20]. Since TDMAP contains nitrogen in its molecular structure, nitrogen incorporation into the phosphate matrix was considered to be advantageous. However, when O_2 plasma was used after TDMAP, nitrogen-free magnesium phosphate films were deposited. This is believed to be because the nitrogen in TDMAP is completely removed by the O_2 plasma. To overcome this problem, we subsequently developed a new ALD process for a magnesium phosphorous oxynitride (MgPON), in which double N_2 plasma processes are applied in each ALD cycle [21]. The deposited film contained ~10% nitrogen, and exhibited an ionic conductivity of 1.2 × 10^{-6} S/cm at 500 °C, which is 7.5 times higher than that of the ALD magnesium phosphate film. However, the MgPON film also contained more than 10% residual carbon, indicating that incomplete chemical reactions take place in the ALD process. Therefore, it is necessary to develop another process to effectively introduce nitrogen into the phosphate matrix with negligible impurities. Shibata et al. reported a thermal ALD for the deposition of LiPON, based on the nitriding of LiO^tBu by NH_3 and the weak oxidation of TDMAP by O_2 [22]. The deposited film showed increased ionic conductivity and a nitrogen content of several percent. However, the growth was only possible at 400-500 °C, which is well above the thermal decomposition temperature of LiO^tBu, putting in doubt the saturation behavior of this process.

Here, we report plasma-assisted ALD growth and various characterizations of lithium phosphate and LiPON films using LiO^tBu and TDMAP precursors. In preliminary experiments, it was found that nitrogen cannot be doped into lithium phosphate films when using O_2 plasma after TDMAP, which is similar to the case for ALD magnesium phosphate processes. This is the underlying motivation for the present study. To achieve the effective doping of nitrogen into the phosphate matrix, the ALD process was carefully investigated using different plasma reactants (O_2, Ar, and NH_3) at deposition temperatures ranging from 220 to 300 °C. We demonstrated how plasma reactant and deposition temperature affect the molecular structure, chemical bonding states, and transport properties of the deposited lithium phosphate and LiPON films. The ALD growth

mechanisms appropriate for obtaining high-performance Li SSE thin films are also discussed.

2. Experimental Section

Lithium phosphate and LiPON films were deposited on Si, SiO_2-covered Si, Pt-coated Si, and quartz substrates, where each substrate was used for a specific characterization method. The substrates were cleaned by acetone and ethanol ultrasonication, followed by plasma ashing in O_2 atmosphere to remove any remaining contaminant species. The substrates were then introduced into an ALD system (SPLEAD Co. Ltd.), in which the base pressure was less than 10^{-2} Pa, and a process pressure of 30 Pa was maintained via an Ar carrier gas flow with 40 sccm. The deposition chamber is schematically illustrated in Figure 1a. The films were deposited at deposition temperatures T_d, ranging from 220 to 300 °C, using LiO^{t}Bu and TDMAP (Japan Advanced Chemicals Ltd.) as the Li and P precursor sources, respectively. These precursors were delivered to the deposition chamber via a 10 sccm Ar carrier gas flow. O_2, Ar, and NH_3 plasma reactants were produced with the direct plasma configuration, where a 13.56 MHz RF voltage was applied to a showerhead irradiating uniform precursor (oxidant H_2O) and plasma reactant gases to the substrates. To ensure that only radicals reached the substrate surface, an additional RF voltage, at 800 kHz, was applied to the sample stage in synchronization with the plasma processes, as illustrated in Figure 1a. All gas flow rates were controlled by mass flow controllers.

We developed ALD processes based on alternative lithium oxide and phosphate (phosphorus oxynitride) sub-cycles. Figure 1b depicts the time sequence of our ALD processes with different plasma reactants. Each cycle started from a 5 s LiO^{t}Bu pulse followed by a 1 s H_2O pulse to form lithium oxide. After that, a 1 s TDMAP pulse is introduced and 1 s plasma pulse with different reactant gasses is applied to make phosphate or phosphorus oxynitride, with application of RF powers of 30 W to the showerhead and 10 W to the sample stage. The purge time was set at 15 s after each pulse.

To evaluate the growth rate, the thickness of films deposited on SiO_2-covered Si substrates was measured using an optical thickness meter (Otsuka Electronics OPTM-F1) in a wavelength region of from 230 to 800 nm. The crystallinity and density of the films deposited on quartz and Si substrates was measured by X-ray diffraction (XRD) and X-ray reflectivity (XRR), respectively, using a Rigaku SmartLab. The film density was estimated from the fitting of XRR curves to theoretical curves, calculated based on a multi-layer model. The morphology of the films deposited on Si substrates were evaluated by atomic force microscopy (AFM) using a Seiko Instruments Nano Navi E-sweep. The chemical bonding state and composition of the films deposited on Si substrates were analyzed by Hard X-ray photoelectron spectroscopy (HAXPES) using an Ulvac

PHI Quantes. Survey and high-resolution core-level spectra were collected using a monochromatic Cr Ka X-ray source. An energy of C 1s peak (284.6 eV) was used for binding energy calibration. Fourier transform infrared spectroscopy (FTIR) measurements were carried out to analyze the chemical bonding state of the films deposited on 100-nm thick Pt coated Si substrates, in an attenuated total reflectance mode, using a Thermo Fisher Scientific iS5 in a wavenumber region of 500-4000 cm^{-1}, with a 2 cm^{-1} resolution.

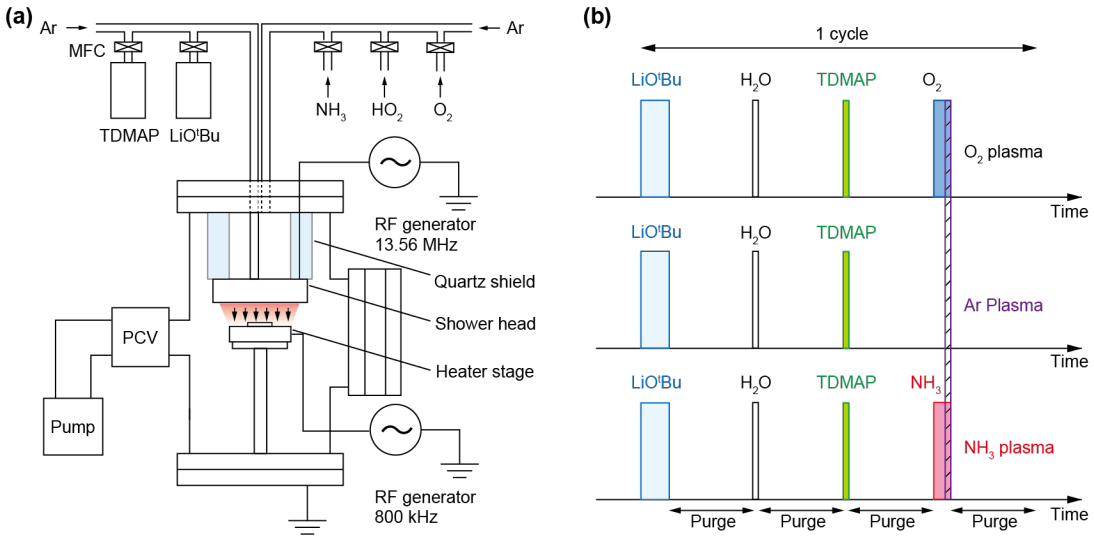

Figure 1. (a) Schematic of the ALD system used in this study. The pressure during deposition is controlled by a pressure control valve (PCV). All gas flow rates were controlled by mass flow controllers (MFCs). Two RF generators were used for producing plasma reactants and ensuring that only radicals reached the substrate surface. (b) Time sequence of one ALD cycle with different plasma reactants.

The transport characteristics were evaluated by electrochemical impedance spectroscopy (EIS) using a Solartron 1260 analyzer, equipped with a 1296 dielectric interface, in a frequency range of from 1 MHz to 0.1 Hz, with an AC amplitude of 5 mV and current-time (*I-t*) measurements using a Keysight B2900. For this measurement, cross-point structured impedance cells with Au electrodes were fabricated on quartz substrates, with a junction area ranging from 0.1 × 0.1 to 2 × 2 mm^2. First, 5-nm thick Ti and 50-nm thick Au were deposited, by electron-beam (EB) evaporation, as the adhesion layer and the bottom electrode. Then, a 50~70 nm thick lithium phosphate or LiPON film was deposited on the Au bottom electrode by ALD. Finally, 50-nm thick Au was EB deposited as the top electrode. The cells were not exposed to air after the ALD deposition, so as to avoid oxidation and contamination of the ALD grown films. The EIS measurements were carried out in an Ar filled glovebox, with < 0.2 ppm of O_2 at a pressure of 7.5

$\times 10^4$ Pa. During the measurements, the substrate temperature T_S was controlled from 25 to 65 °C, in increments of 10 °C.

3. Results and Discussion

The growth behaviors of films deposited on SiO_2/Si substrates by ALD processes with different plasma reactants are summarized in Figure 2. Here, Ar plasma is taken to mean that the RF voltage was applied in an Ar atmosphere without additional reactant gases, as illustrated in Figure 1b. Figure 2a and 2d show the growth rate (growth-per-cycle) plotted as a function of the LiO^{t}Bu pulse time up to 6 s, with O_2 and Ar plasma reactants, respectively, evaluated for T_d of 300 °C. For both plasma reactants, the growth rate increased with the pulse time and became almost constant after 5 s, indicating a self-limiting behavior. The growth rate increased to ~0.75 Å/cycle for O_2 plasma, similar to that observed for lithium phosphate films deposited by thermal ALD processes using LiO^{t}Bu and TMP [23]. In contrast, with Ar plasma, the growth rate considerably increased to ~1.8 Å/cycle, which is more than two times higher than with O_2 plasma. From these results, we set the LiO^{t}Bu pulse time to 5 s for all the depositions. Figure 2b and 2e plot the film thickness as a function of the number of ALD cycles up to 400 cycles, with O_2 and Ar plasma, respectively, for T_d of 300 °C. It is clearly seen that film thickness is linearly proportional to the number of ALD cycles. Figure 2c and 2f show the T_d dependence of the growth rate of the films deposited with O_2 and Ar plasma, respectively. They exhibited the opposite tendency with T_d: the growth rate with O_2 plasma increased with a decrease of T_d, whereas the growth rate with Ar plasma decreased. The T_d dependence with Ar plasma is similar to that of thermal ALD lithium phosphate films using LiO^{t}Bu and TMP [24]. Figure 2g plots the growth rate with NH_3 plasma as a function of the flow rate of NH_3 gas for T_d of 300 °C, showing a slight increase up to 20 sccm. The film deposited with NH_3 plasma also exhibited linear thickness dependent on the number of ALD cycles, as shown in Figure 2h, which is similar to other plasma reactants. However, the T_d dependence of the growth rate was significantly different from that with Ar plasma. The growth rate increased slightly with a decrease of T_d, reaching ~2 Å/s at 220 °C, as shown in Figure 2i. This suggests that the growth mechanism is significantly altered when NH_3 plasma is introduced. Note that the growth rate also did not change with the pulse times of both H_2O and TDMAP, as shown in Figure S1 of Supporting Information, which indicates the self-limiting behavior of all the ALD processes.

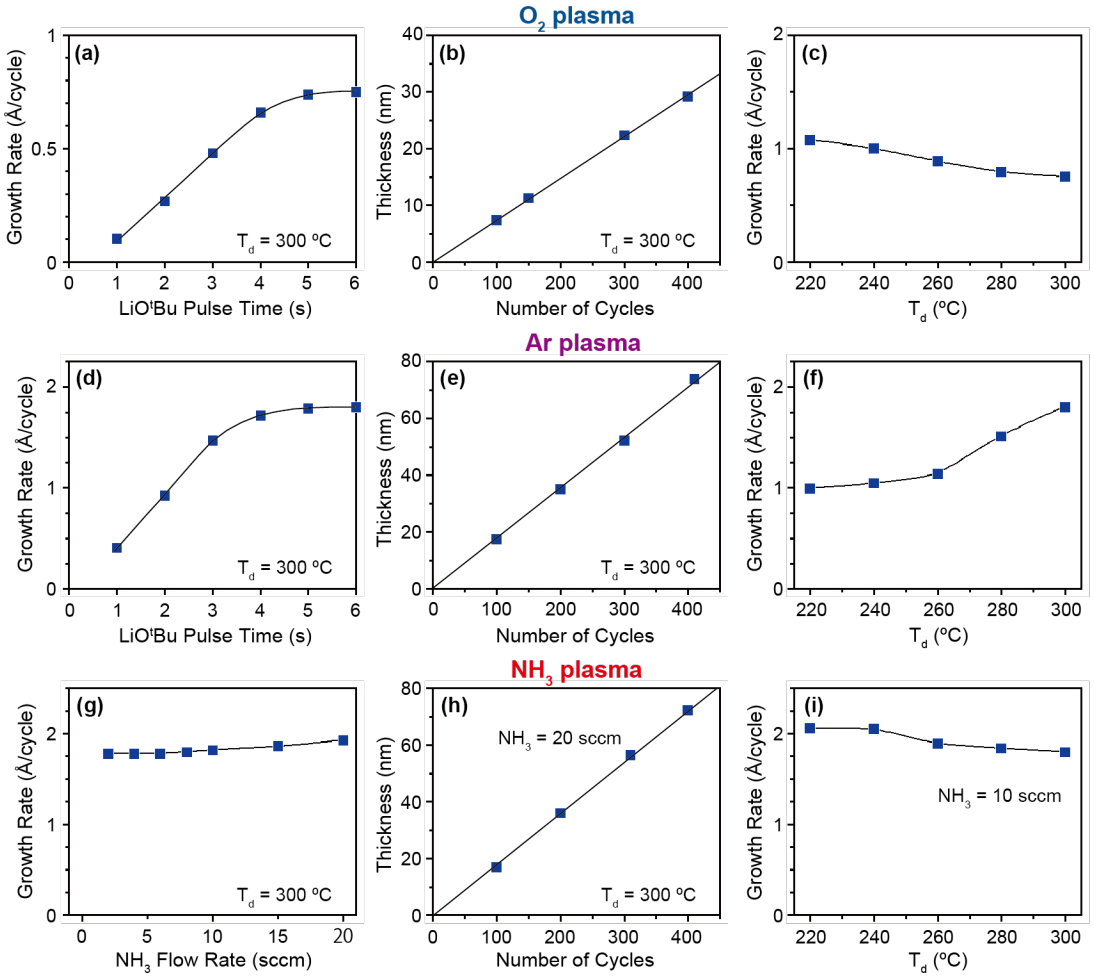

Figure 2. Growth behaviors of films deposited with different plasma reactants. (a)-(f) Growth rates versus LiO^{t}Bu pulse time, film thickness versus number of ALD cycles, and growth rate versus T_d, measured with O_2 and Ar plasma, respectively. (g)-(i) Growth rate versus NH_3 flow rate, film thickness versus number of ALD cycles, and growth rate versus T_d, measured with NH_3 plasma. The solid curves are a guide for the eye.

The effects of plasma reactants on the crystallinity and surface morphology were examined by XRD and AFM measurements. For these measurements, films deposited at 220 and 300 °C for 300 cycles were prepared. The NH_3 flow rate was set at 20 sccm for NH_3 plasma. The blue curve of Figure 3a represents an XRD pattern of a film deposited at 220 °C with O_2 plasma. The films were polycrystalline in nature, with diffraction peaks at 23.5° and 25°, with small peaks at 34° and 37°; these are attributed to the (101), (011), (210)/(020), and (002) planes of lithium phosphate, respectively [25]. Similar diffraction peaks were observed for lithium phosphate films deposited by thermal ALD processes using LiO^{t}Bu and TMP [15]. The film deposited at 300 °C was likely to be more crystallized, evidenced by slightly developed peaks at 34° and 37° in the red curve. In

contrast, films deposited with Ar and NH_3 plasma did not show any crystalline peaks for either deposition temperatures, as shown in Figure 3b and 3c. This suggests that Ar and NH_3 plasma produce amorphous films for all the deposition temperatures examined.

Figure 3d shows an AFM image of film deposited at 220 °C with O_2 plasma, measured in a non-contact mode using a Si cantilever. The film showed surface morphology of randomly piled-up of crystal grains, each with a size of more than several tens of a nanometer. The root mean square (RMS) was estimated to be 1.15 nm. The grain sizes became larger for film deposited at 300 °C, as shown in Figure 3g. The RMS was estimated to be 2.09 nm, indicating that the film surface becomes rougher at higher deposition temperatures. This is consistent with the XRD result, which showed that the film was more crystalline at higher deposition temperatures. With Ar plasma, the surface roughness was significantly reduced, as shown in Figure 3e and 3h. The RMS was estimated to be ~0.35 nm for both deposition temperatures. The AFM images still show granular features, but their size decreased to l0 - 20 nm. With NH_3 plasma, the film surface became flat and the RMS was further reduced to ~0.2 nm for both deposition temperatures, as seen in Figure 3f and 3i, which is typical morphology for an amorphous film. These results indicate that the crystallinity and surface morphology depend strongly on the plasma reactant and slightly on the deposition temperature. Of the plasma reactants examined, NH_3 plasma alone resulted in smooth and uniform film surfaces.

HAXPES is a powerful tool for evaluating the chemical bonding state of films that are several to ten times deeper than conventional XPS, due to the high-energy X-ray excitation. According to the photoelectron detection intensity curve, assuming a homogeneous Li oxide layer, as calculated by Fantin et al., the sampling depth at which the intensity is measured is estimated to be ~20 nm for our measurement configuration (with a 90° sample tilt angle) [26]. Figure 4a represents survey spectra measured for as-deposited films with three plasma reactants at T_d of 300 °C. It was not possible to avoid oxidation and carbonization of the film surface, even though the films were only exposed to air for a short period of time (less than 1 min.) when being transferred from the ALD system to the XPS apparatus. Peaks were observed at binding energies of ~530, ~284, ~133, ~55 eV for the film deposited with O_2 plasma, which are assigned to O 1s, C 1s, P 2p, and Li 1s, of lithium phosphate, respectively [23]. In addition to these peaks, a peak attributed to N 1s appeared at ~398 eV for the films deposited with Ar and NH_3 plasma, which indicates the existence of nitrogen doped in the lithium phosphate, and which corresponds to the formation of LiPON.

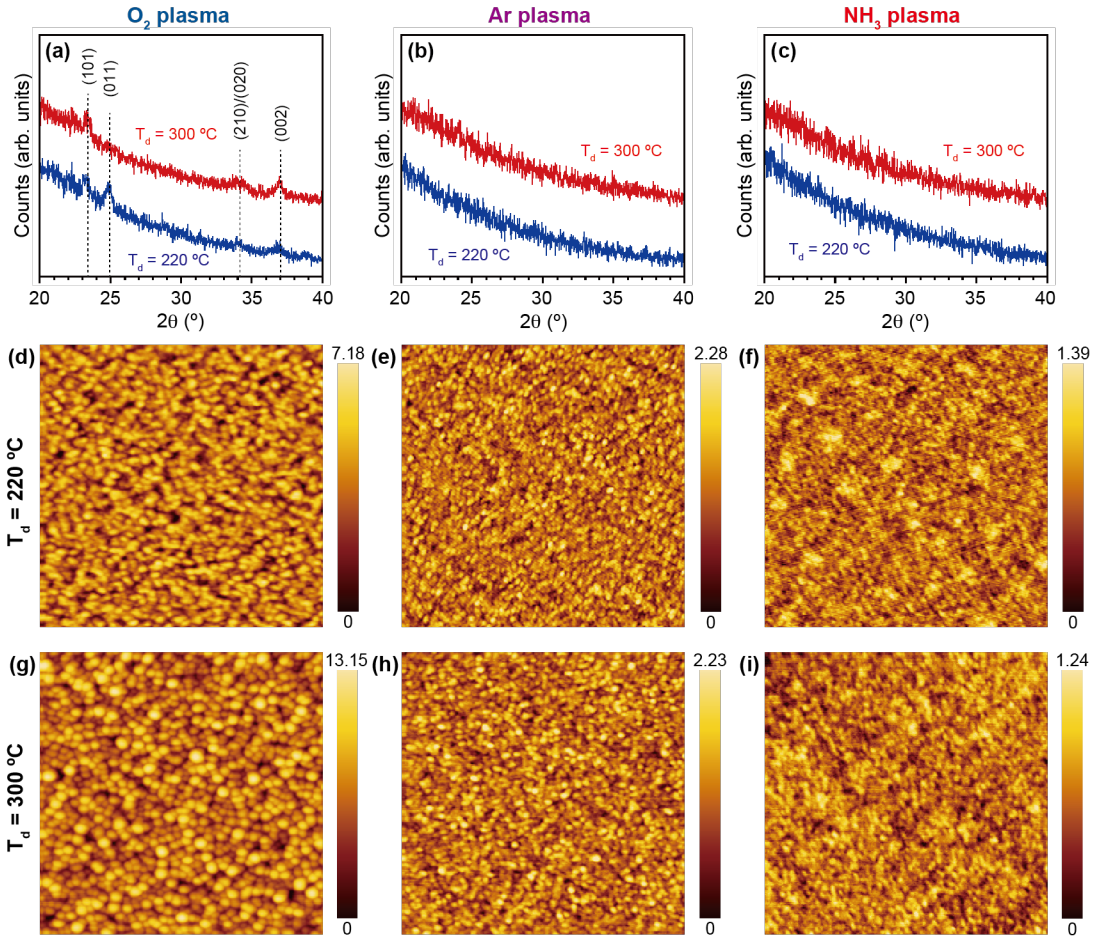

Figure 3. XRD patterns measured for films deposited at 220 and 300 °C for 300 cycles with (a) O_2, (b) Ar, and (c) NH_3 plasma. Corresponding AFM images (1 μm × 1 μm) measured for films deposited at 220 °C with (d) O_2, (e) Ar, and (f) NH_3 plasma, and at 300 °C with (g) O_2, (h) Ar, and (i) NH_3 plasma.

Figure 4b-4g show high-resolution core-level spectra of O 1s and N 1s for different plasma reactants. When nitrogen is substituted for oxygen sites in lithium phosphate, nitrogen breaks P-O and Li-O bonds and replaces the bridging oxygen (BO) bonds in P-O-P bonds and the non-bridging oxygen (NBO) in Li-O-P and P=O bonds, forming doubly-bound nitrogen (P=N-P) and triply-bound nitrogen (P-N<P_2), respectively [27]. The O 1s and N 1s spectra were found to contain two peaks, each with a small peak on the high-binding energy side of the main peak. The O 1s peak can be deconvoluted into two peaks located at 533.2 and 531.8 eV, as shown in Figure 5b-5d. These peaks are attributed to the BO and NBO respectively [28]. The film deposited with O_2 plasma did not show any nitrogen-related peaks, indicating that TDMAP was completely oxidized by O_2 plasma and lithium phosphate is formed. On the other hand, the films deposited with Ar and NH_3 plasma exhibited a N 1s peak, which can be deconvoluted into two peaks located at 398.6 and

397.1 eV, as shown in Figure 4e-4g. The peak on the low-binding energy side corresponds to the doubly-bound nitrogen, and the other peak is assigned to the triply-bound nitrogen. The N 1s peaks developed with increasing NH_3 flow rate, whereas the O 1s peaks reduced. The O 1s spectra evidence a low amount of BO in the phosphorus oxynitride matrix (< 10%). The N 1s spectra indicate that nitrogen is mainly doubly bonded and is related to the formation of bridges between phosphate units.

The high-resolution core-level spectra of P 2p and Li 1s are shown in Figure S3 of Supporting Information. Both spectra show a single peak at 132.9 and 54.9 eV respectively, which is agreement with values previously observed for sputtered LiPON [29] and ALD LiPON [15] [17] films. The P 2p peak was not fitted to identify the spin orbit splitting of the 2p orbital, but it showed symmetric profiles. There was no obvious shift of these Li 1s and P 2p peaks with different plasma, which indicates a single chemical environment for these elements regardless of the plasma reactants used.

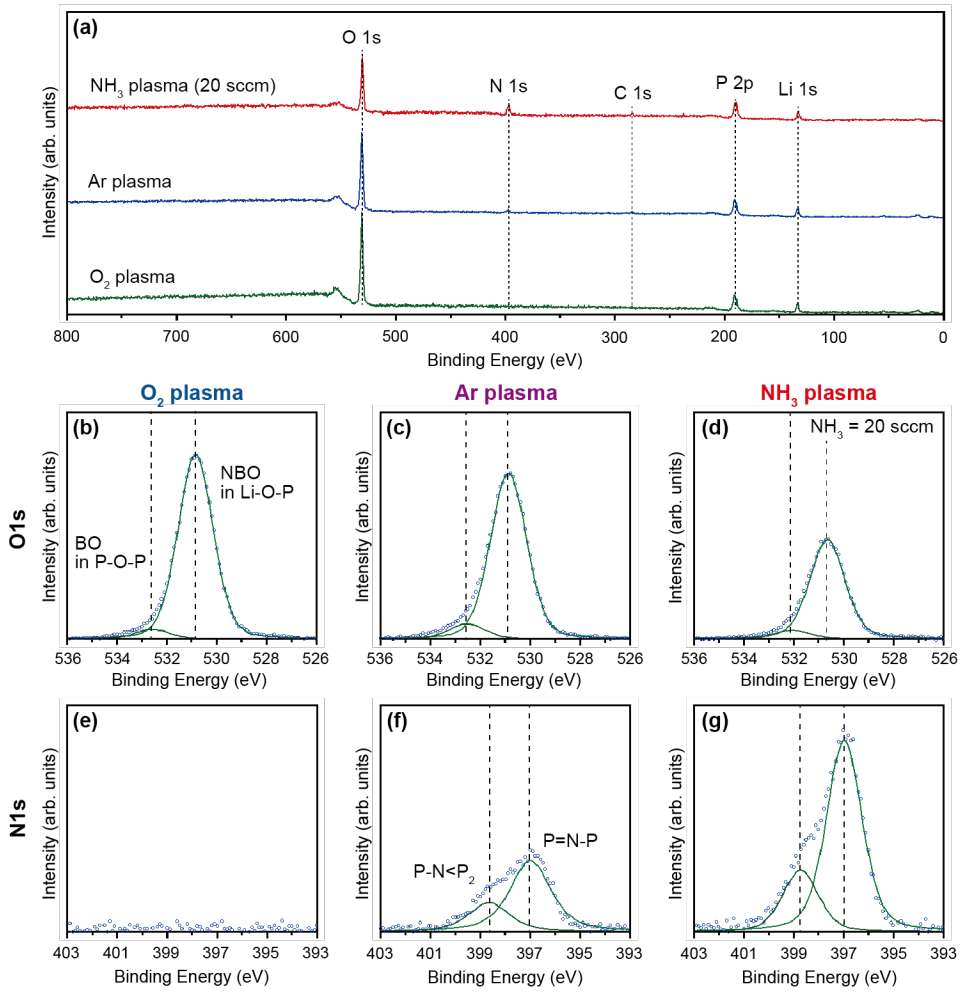

Figure 4. HAXPES results measured for as-deposited ALD films deposited at 300 °C with different plasma. (a) Survey spectra. (b-g) High-resolution core-level spectra of O 1s and N 1s (rows) for different plasma reactants (columns). Spectra are deconvoluted into multicomponent peaks.

The chemical bonding states in the deposited films were also be examined by FTIR spectroscopy. Figure 5 shows FTIR spectra for films deposited on Pt/Si substrates, with the respective plasma reactants at T_d of 300 and 220 °C respectively. With O_2 plasma, a large and sharp peak was observed at 1130 cm^{-1} for both deposition temperatures, as seen in Figure 5a. This peak is attributed to the symmetric stretching vibration (ν_a) of PO_3^{2-} ions in the pyrophosphate ($Li_4P_2O_7$) [30]. The pyrophosphate is based on phosphate dimers, where two phosphate groups share a BO [31]. In addition, two peaks were observed at 532 and 624 cm^{-1}, which peaks are associated with the characteristic vibrational mode (ν) of Li-O bonds and the bending vibration (δ) of O-P-O bonds, respectively [32] [33]. A small peak appeared at ~950 cm^{-1}, corresponding to the asymmetric stretching vibration (ν_{as}) of P-O-P bonds [31]. The films also exhibited small peaks at around 1455 cm^{-1}, which peaks are related to ν_{as} of CO_3^{2-} (carbonate) ions [34]. This indicates that lithium carbonate (Li_2CO_3) was formed, probably due to exposure in air during the film's transportation from the ALD system prior to FTIR measurements. The spectral shape did not change with deposition temperature variation.

With Ar plasma, the deposited films exhibited a broad peak at 1130 cm^{-1}, with a shoulder on the high wavenumber side, as shown in Figure 5b. The shoulder looks to be located at around ~1190 cm^{-1}, which position is outside of the spectral range (1200-1300 cm^{-1}) expected for ν_{as} of PO_2^- ions in the metaphosphate [32] [33]. Carrillo Solano et al. have investigated how specific structural units of LiPON are detected with X-ray photoemission and infrared spectroscopies [31]. Although the peak at ~1190 cm^{-1} was slightly higher than the position (1150 cm^{-1}) observed for them, it can be assigned to ν_s of N-P-O bonds involving in the bridging of nitrogen. The appearance of this peak indicates the incorporation of nitrogen into the phosphate matrix, which is consistent with the HAXPES result. The spectral shape did not change with deposition temperature variation, although the relative intensity between the peaks of PO_3^{2-} ions and N-P-O bonds changed slightly. When NH_3 was used, the presence of such bridging nitrogen was enhanced. The film deposited at 300 °C showed that the peak intensity of N-P-O bonds becomes higher than that of PO_3^{2-} ions with an increase of NH_3 flow rate, as seen in Figure 5c. At a NH_3 flow rate of 20 sccm, a small peak also appeared at ~850 cm^{-1}. Du and Holzwarth have computed the molecular structure and related vibrational spectra of various LiPON compositions [35]. According to their calculations, a peak at 850 cm^{-1} is attributed to ν_{as} of P-N-P bridges in a chain structure with a -P-N-P-N- backbone,

which also evidences the incorporation of nitrogen into the phosphate matrix. A similar peak was observed in MOCVD LiPON films [13] and ALD MgPON films deposited with N_2 plasma [21]. The peak around 550 cm^{-1} from Li-O bonds was significantly broadened, which is probably due to changes introduced in the chemical environment around Li ions due to nitrogen incorporation. Note that no absorption peak related to carbonate ions was observed in the films deposited with Ar and NH_3 plasma, contrary to the films deposited with O_2 plasma. This suggests the improved stability under atmospheric conditions for films deposited with Ar and NH_3 plasma. Figure S2 of Supporting Information shows an FTIR spectrum of the film deposited at 220 °C with NH_3 plasma. The spectral feature is almost the same as that of the film deposited at 300 °C, indicating that the chemical bonding state is independent of the deposition temperature. A small 'shoulder' was always observed at 1020 cm^{-1}, which corresponds to ν_{as} of PO_4^{3-} ions [31]. This implies the presence of a small amount of orthophosphate for all plasma processes.

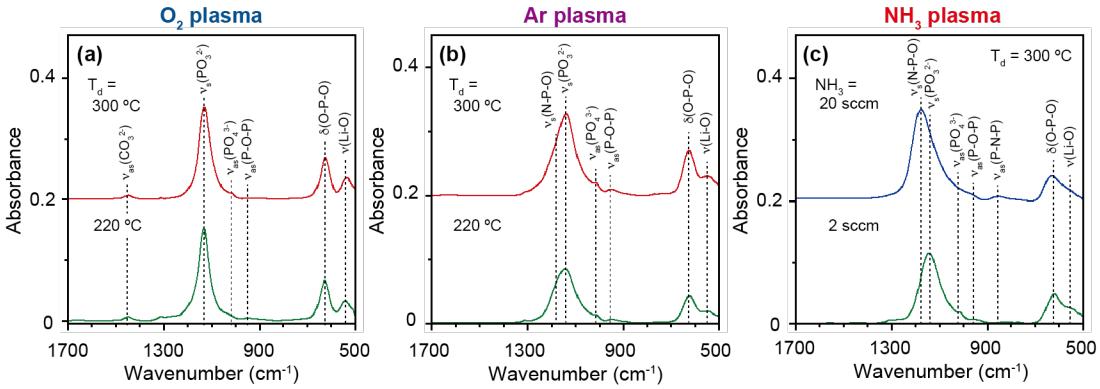

Figure 5. FTIR spectra measured for films with (a) O_2 plasma and (b) Ar plasma, deposited at 300 and 220 °C, and (c) films with NH_3 plasma for different NH_3 flow rates, deposited at 300 °C.

From HAXPES quantifications, the elemental composition of the films deposited at 300 °C with different plasma reactants were calculated, and the results are summarized in Table I. The uncertainty in determining the atomic composition is estimated to be less than ±0.5%. The ALD process with O_2 plasma produced $Li_{3.3}PO_{3.4}$, which composition is more slightly Li rich and O deficient than the stoichiometric lithium phosphate (Li_3PO_4). The process with Ar plasma resulted in an already nitrogen-contained lithium phosphate film, that is LiPON. The elemental composition was estimated to be $Li_{2.8}PO_{2.9}N_{0.2}$. At increased NH_3 flow rates, the composition of nitrogen increased, while that of oxygen decreased. At an NH_3 flow rate of 20 sccm, the film exhibited a composition of $Li_{2.5}LiPO_{1.9}N_{0.8}$, the Li content of which is 25% higher than found in the stoichiometric pyrophosphate LiPON (Li_2PO_2N). This higher Li content can be explained by a mixture of pyrophosphate and orthophosphate ($Li_6P_2O_5N_2$) [31]. There was a small amount (less

than a few %) of carbon in the deposited films, which showed that the employed processes can greatly reduce residual carbon as compared to thermal ALD LiPON film [16]. The elemental composition of films deposited at 220 °C are summarized in Table S-I of Supporting Information. The composition did not change significantly with decreased deposition temperatures, although there was a slight increase in the amount of residual carbon (up to 4.6%), particularly for NH_3 plasma processes. This suggests that incomplete chemical reactions may occur during the ALD process with plasma at higher NH_3 flow rates, which is significant for lower deposition temperatures. Further research is needed to elucidate the effect of higher NH_3 flow rates on chemical reactions and the resultant composition.

Table I Elemental composition of films deposited at 300 °C with different plasma reactants, determined by HAXPES

Plasma reactant	Atomic composition (%)					Composition relative to P excluding C
	Li	P	O	N	C	
O_2	42.6	13.0	43.0	0	1.4	$Li_{3.3}PO_{3.4}$
Ar	39.5	14.4	41.3	2.8	2.0	$Li_{2.8}PO_{2.9}N_{0.2}$
NH_3 (20 sccm)	39.3	15.6	28.9	13.2	3.0	$Li_{2.5}PO_{1.9}N_{0.8}$

Figure 6 plots the nitrogen composition as a function of the NH_3 flow rate for the LiPON films deposited at 300 °C, which were evaluated from HAXPES analyses. Note that the flow rate of 0 sccm corresponds to the film deposited with Ar plasma. With increasing NH_3 flow rate, the nitrogen composition increased and then asymptotically approached ~13% up to 20 sccm. This result indicates that the NH_3 plasma processes starting from Ar plasma could deposit LiPON films with a controlled nitrogen composition. If the NH_3 flow rate was further increased, the nitrogen composition saturated at the 13 % level. Hence, such nitrogen content is considered the maximum composition possible using current ALD processes. Note that if even a small amount of O_2 gas was introduced with NH_3 plasma, nitrogen cannot be doped into the phosphate matrix at all. This means that TDMAP is highly oxidizable and thus no O_2 plasma is needed to form the phosphorus oxynitride matrix.

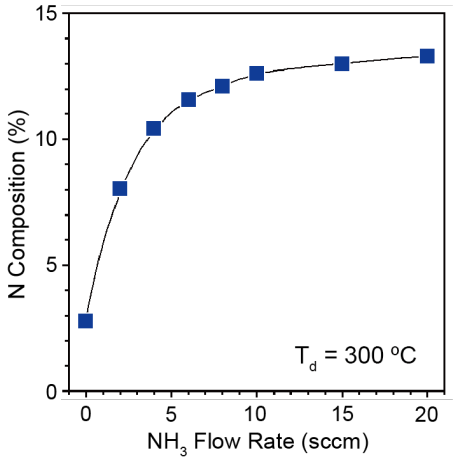

Figure 6. Nitrogen Composition plotted as a function of NH_3 flow rate, evaluated from HAXPES analyses for films deposited at 300 °C with Ar and NH_3 plasma. The solid curve is a guide for the eye.

The electrical conductivity of the lithium phosphate and LiPON films deposited with different plasma reactants was evaluated by EIS and *I-t* measurements. Figure 7a plots EIS data measured at 25 °C for lithium phosphate and LiPON films deposited at 300 °C with O_2 plasma (open squares) and Ar plasma (open circles), respectively. The EIS data consist of an intercept on the real axis at high frequency, two semicircles at the medium frequency range, and a vertical response coming from the electrode polarization due to the ionic blocking contact. Such features are typically representative of ionic conductors, if the measurement is applied for an ionic conductor in an open circuit with ion blocking electrodes. Although the EIS data is likely to show a single semicircle, the analysis indicated that they are actually composed of two semicircles. We see that the semicircle of the LiPON film deposited with Ar plasma became smaller by more than one order of magnitude, compared to the lithium phosphate film deposited with O_2 plasma. Figure 7a also displays curves fitted to the EIS data, based on an equivalent circuit model, as shown in the inset. The model consists of four series components; one contact ohmic resistance (R_o), which was attributed to the high-frequency limiting resistance of the electrode, two parallel resistors and constant-phase elements (CPE) in the middle frequency range, with one (R_B and CPE_B) corresponding to the bulk of the lithium phosphate or LiPON film and the other (R_I and CPE_I) corresponding to the resistive reaction layer between the deposited film and the Au electrode, and finally a single CPE (CPE_{block}) corresponding to electrode polarization in the low-frequency region. The last component can be attributed to the formation of an electrochemical double layer at both electrode interfaces [36].

Figure 7b shows EIS data with fitting curves, measured at 25 °C, for LiPON films deposited

at 300 °C with NH_3 plasma of different NH_3 flow rates. The semicircle became smaller with an increased NH_3 flow rate, suggesting that the conductivity increased with increased NH_3 flow rates and thus with increased nitrogen compositions. The ionic conductivity σ of the measured films was simply calculated by substituting the bulk resistance into the equation: $\sigma = d/(AR_B)$, where d is the thickness of the deposited film, and A is the geometric junction area of the impedance cell. The Arrhenius plot of the ionic conductivity, calculated for films deposited with different plasma reactants, is plotted in Figure 7c. The lithium phosphate film deposited with O_2 plasma exhibited an ionic conductivity of $1.75 \pm 0.52 \times 10^{-9}$ S/m at 25 °C, which increased to $1.16 \pm 0.3 \times 10^{-7}$ S/cm at 65 °C. This conductance level is similar to the previously reported values of ALD lithium phosphate films [18] [23]. If Ar plasma was used, the ionic conductivity significantly increased to $1.34 \pm 0.43 \times 10^{-7}$ S/cm at T_S of 25 °C, which is two orders of magnitude higher than that of the lithium phosphate film deposited with O_2 plasma. The ionic conductivity increased to $2.95 \pm 1.18 \times 10^{-6}$ S/cm at 65 °C. This conductivity level is slightly higher than that of thermal ALD films, with a similar nitrogen content, deposited using LuO^tBu and TMP [15]. When NH_3 plasma was used with an NH_3 flow rate of 20 sccm, corresponding to the nitrogen composition of 13.2 %, the ionic conductivity further increased to $1.65 \pm 0.42 \times 10^{-6}$ S/cm at 25 °C, which is one order of magnitude higher than that of the film deposited with Ar plasma. This value is the highest conductivity of all ALD LiPON films reported to date. As T_S increased to 65 °C, the ionic conductivity was increased to $3.21 \pm 0.56 \times 10^{-5}$ S/cm. The activation energies (E_a) for the ionic conductivity were also evaluated by using the Arrhenius equation: $\sigma T = B \exp[-E_a/(k_B T)]$, where B is a pre-exponential factor, T is the absolute temperature, and k_B is the Boltzmann's constant. From linearly fitting to the experimental data, the E_a was estimated to be 0.91 eV for the lithium phosphate film deposited with O_2 plasma and 0.66 eV for the LiPON films with Ar and NH_3 plasma, as shown in Figure 7c. These values are somewhat higher than the values reported for other ALD lithium phosphate films (0.51 eV) [23] and slightly higher than the values for other LiPON films (0.55 eV) [16] respectively.

Figure 7d plots the ionic conductivity as a function of the nitrogen composition, evaluated at 25 °C, for LiPON films deposited at 300 °C with Ar and NH_3 plasma. There is an exponentially increasing relationship of the ionic conductivity with the nitrogen composition. The electronic conductivity was evaluated at 25 °C by measuring an *I-t* response curve under an application of a constant 1 V bias to an impedance cell with a 70 nm-thick LiPON film. The result is shown in Figure 7e. The measured current rapidly decayed to 0.1 nA within one minute and then gradually decreased over time. This gives rise to an electronic conductivity (σ_e) of $\leq 2.0 \times 10^{-12}$ S/cm, which is nearly six orders of magnitude lower than the ionic conductivity. Thus, we conclude that LiPON

film deposited with NH_3 plasma is a highly ionic conductor and an electronically insulating electrolyte. As the deposition temperature was decreased to 220 °C, the ionic conductivity of the LiPON film deposited with NH_3 plasma decreased by a half to one third, and the E_A slightly increased to 0.73 eV, as shown in Figure 7f. The nitrogen composition estimated by HAXPES remained almost unchanged for T_d of 300 and 220 °C (see table I and S-I), but the ionic conductivity apparently decreased with decreasing deposition temperature. In contrast, lithium phosphate and LiPON films deposited with O_2 and Ar plasma exhibited similar σ and E_a values for T_d of both 300 and 220 °C, as shown in Figure S4 of Supporting Information. This indicates that the temperature effect of NH_3 plasma on ionic conductivity is somewhat different from those of O_2 and Ar plasma.

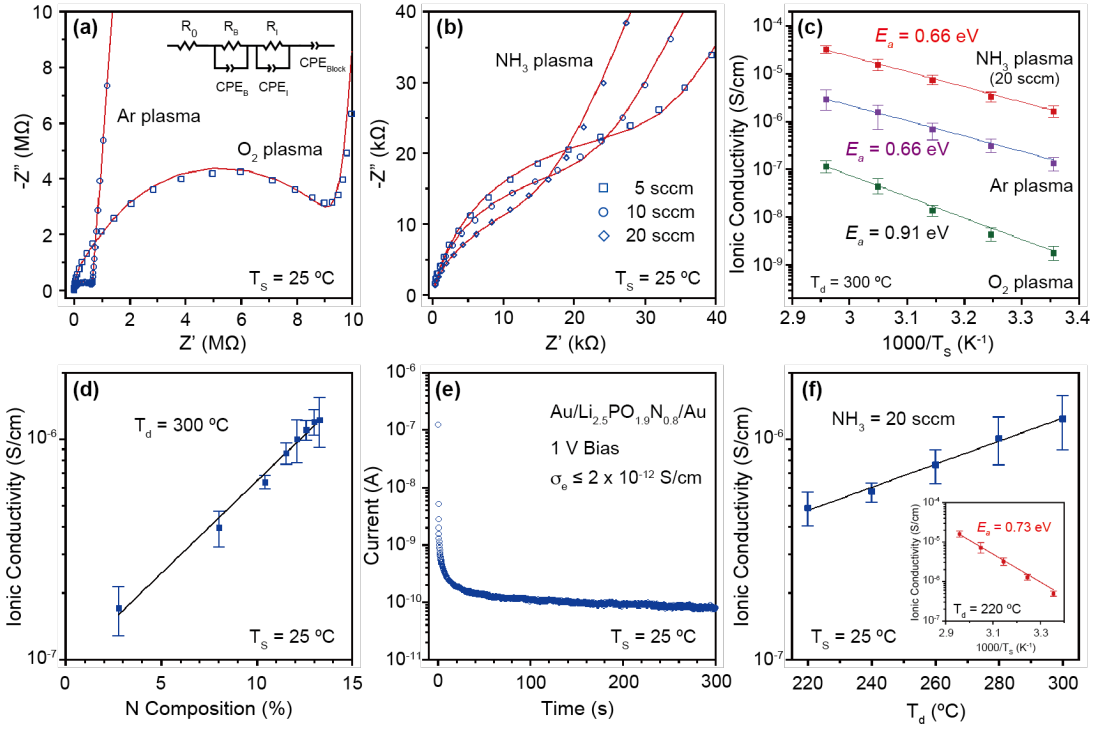

Figure 7. (a) EIS plots measured at 25 °C for Au/LiPON/Au impedance cells with films deposited at 300 °C with O_2 plasma (open squares) and Ar plasma (open circles), with fitting curves based on the equivalent circuit model as illustrated in the inset. (b) EIS plots measured for cells with films deposited with NH_3 plasma of different NH_3 flow rates, with fitting curves. (c) Arrhenius plots of the ionic conductivity for films deposited at 300 °C with three plasma reactants. The solid lines are fitted to the experimental data using the Arrhenius equation. (d) Ionic conductivity plotted as a function of nitrogen composition. (e) *I-t* response measured for an impedance cell under a 1 V constant bias, showing the low electronic conductivity of an LiPON film deposited with NH_3 plasma. (f) Ionic conductivity plotted as a function of deposition temperature, measured for LiPON films deposited with NH_3 plasma. The inset shows an Arrhenius plot for a film deposited at 220 °C.

In general, phosphate glass (P_2O_5) consists of PO_4 tetrahedra connected through P-O-P bonds, resulting in a polymeric structure [37]. The PO_4 tetrahedra are accompanied with their adjacent counterparts by three vertices corresponding to $P\text{-}O^-$ bonds, while the remaining vertex is occupied by a P=O bond [38] [39]. As a result, the main structure of the phosphate is composed of BO in P-O-P bonds. If Li atoms are added to this phosphate structure, the structure is de-polymerized by converting the BO to NBO of Li-O-P bonds [40]. The transport of Li ions in this glass structure is considered to originate from thermally activated hopping between NBOs [41] [42]. Such a transport mechanism is mainly attributed to the diffusion of mobile ions through potential minima in the glassy network. The results of XRD and FTIR indicate that films with O_2 plasma formed a relatively well-arranged pyrophosphate, interconnected by Li-O-P and P-O-P chains. On the other hand, films with Ar or NH_3 plasma exhibited an amorphous phosphorus oxynitride consisting of a disordered mixture of pyrophosphates and orthophosphates. Such matrix can create more space in the phosphorus oxynitride network, which acts as conduction pathways for Li ions. Therefore, the higher conductivity observed for LiPON films deposited with NH_3 plasma is attributed to the enhanced hopping conduction of Li ions in a less dense phosphorus oxynitride matrix. The higher Li content may also contribute to the high ionic conductivity [31].

To confirm our hypothesis, XRR measurements were performed to determine the density of films deposited at 300 and 220 °C, with three plasma reactants. The measured XRR curves were fitted with theoretical curves calculated using a multi-layer model, as shown in Figure S5 of Supporting Information. The results are summarized in Figure 8. With O_2 plasma, the densities were estimated to be 2.15 and 2.18 g/cm^3 for the lithium phosphate films deposited at 300 and 220 °C, respectively. These values are 15% lower than the theoretical value (2.54 g/cm^3) of a crystalline Li_3PO_4 structure. The similar density values for both deposition temperatures are consistent with the similar FTIR spectra of Figure 4a. Therefore, films deposited at the two deposition temperatures both exhibited similar conductivity values, as shown in Figure S3a. When Ar plasma was used, the density decreased to 1.92 and 2.0 g/cm^3 for the LiPON films deposited at 300 and 220 °C, respectively. The smaller density at 220 °C may be associated with the development of N-P-O bonds, as seen in Figure 4b. The phosphate matrix is changed to phosphorus oxynitride with a mixture of two phosphates with a slightly lowered density. The ionic conductivity increased significantly when even a small amount (< 3%) of nitrogen was incorporated, but no difference was observed in the deposition temperature range examined, as shown in Figure S3b. When NH_3 plasma was used, considerable nitrogen was incorporated into the phosphorus oxynitride, with a further decreased density. At T_d of 300 °C, the film density was 1.81 g/cm^3,

which is 17% lower than that of lithium phosphate films deposited with O_2 plasma. The phosphorus oxynitride matrix becomes more disordered, which enhances the conductivity of Li ions. The density (1.95 g/cm^3) at T_d of 220 °C was found to be somewhat higher than the density at 300 °C. The denser phosphorus oxynitride may result in lower ionic conductivity, as show in Figure 7f. Thus, the change in density accounts for the origin of the high ionic conductivity of ALD LiPON films.

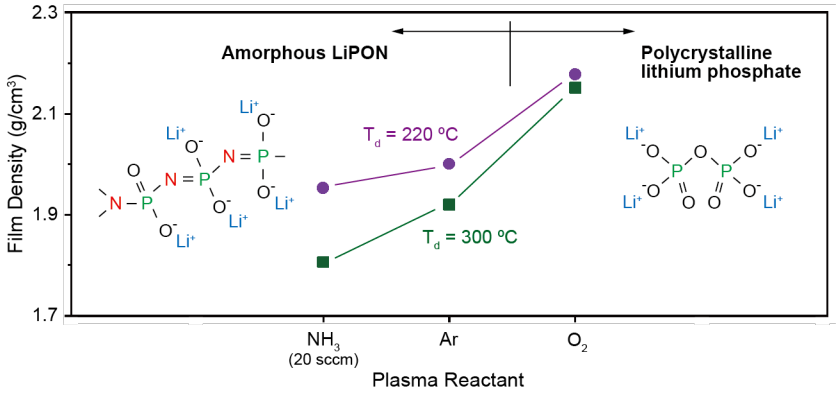

Figure 8. Density of lithium phosphate and LiPON films deposited at 300 and 220 °C with different plasma reactants, evaluated from XRR measurements. The insets illustrate the molecular structures of lithium phosphate (left) and LiPON (right) films.

Finally, we inferred the growth mechanism of our ALD lithium phosphate and LiPON films from the obtained results. Figure 9 shows schematic illustration of the proposed scheme with different plasma reactants for the first ALD cycle. The processes start from the termination with hydroxyl (-OH) groups on the substrate surface by the initial H_2O pulse (Figure 9a). Then, a LiOtBu pulse is introduced to form Li-O units on the surface (Figure 9b). After that, Another H_2O pulse is introduced to loosely bond to the Li-O units. (Figure 9c). Up to this point, the process corresponds to the first half of the process; the Li-O sub-cycle. The latter process consists of a phosphate or phosphorus oxynitride sub-cycle, depending on the plasma reactant. A subsequent TDMAP pulse causes the reaction of TDMAP and H_2O to lead to termination with dimethylamino phosphate ligands (Figure 9d). When O_2 plasma is used, the dimethylamino phosphate ligands are completely removed and the phosphate matrix becomes denser, which leads to cross-linking of the phosphorus atoms. P-O-P and O=P-O bonds are formed, resulting in the formation of polycrystalline pyrophosphates (Figure 9e). Because of the higher densities, the growth rate lowers for lithium phosphate films with O_2 plasma (Figure 2c). Li is bound to some oxygen atoms of the phosphate tetrahedra. When Ar plasma is used, nitrogen is incorporated from the dimethylamino phosphate ligands into some of the cross-linking phosphate network, and nitrogen atoms are

mainly double bonded to form bridges between phosphate tetrahedra. The phosphate matrix becomes phosphorus oxynitride, with an amorphous nature, resulting from a disordered mixture of pyrophosphate and orthophosphate (Figure 9f). Because of the reduced density, the growth rate of LiPON films with Ar plasma considerably increases (Figure 2f), which is advantageous for shortening the deposition time. Finally, when NH_3 plasma is used, lots of nitrogen atoms are incorporated into the cross-linking phosphorus oxynitride network, increasing the number of doubly- and triply-bound nitrogen atoms (Figure 9g). The phosphorus oxynitride matrix is even more disordered and the film density is further decreased. As a consequence, the growth rate increases further with NH_3 plasma (Figure 2i). After the second cycle, the H_2O pulse creates excess H_2O attached to the phosphate and probably forms clusters of water molecules on the top surface, due to the high reactivity of phosphorus with water. This excess water becomes a source of oxygen when Ar and NH_3 plasma are used, and promotes the formation of phosphorus oxynitrides.

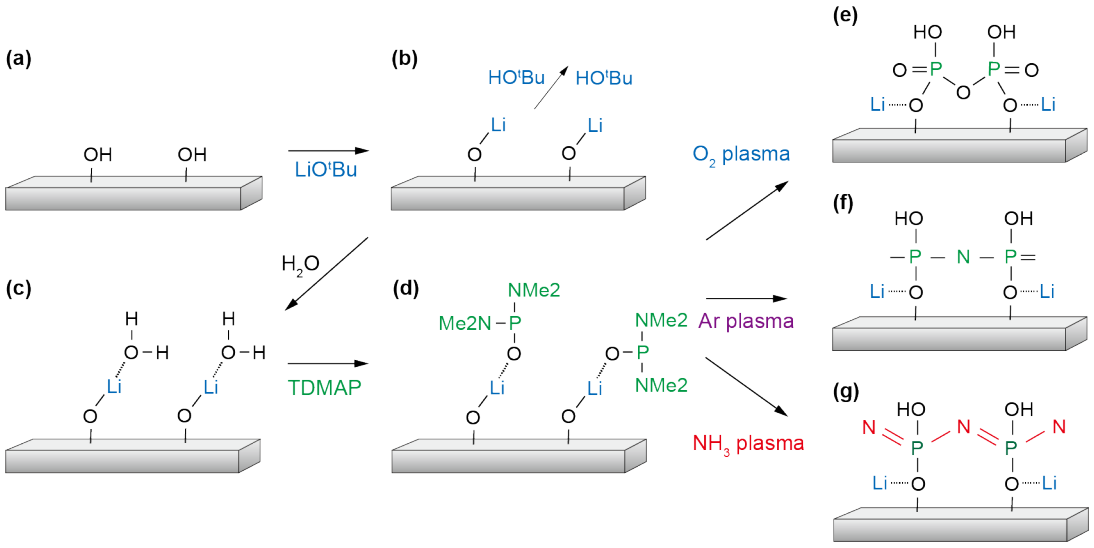

Figure 9. Schematic of the proposed ALD lithium phosphate and LiPON growth scheme with different plasma reactants for the first cycle. (a) Initial surface terminated with hydroxyl groups; (b) Formation of Li-O units after a LiO^{t}Bu pulse; (c) Adsorption of H_2O to the Li-O units by a H_2O pulse; (d) a TDMAP pulse for P incorporation; (e) O_2 plasma to cross-link P atoms and form a dense polycrystalline phosphate matrix; (f) Ar plasma to incorporate a small amount of nitrogen into the phosphate matrix, resulting in amorphous LiPON with a lowered density; (g) NH_3 plasma to increase the nitrogen incorporated into the phosphorus oxynitride, further reducing the density.

It is generally believed that Li is bound to oxygen atoms in phosphate tetrahedra in both phosphorus oxide and oxynitride networks, as shown in Figure 9. The first-principle calculations done by Du and Holzwarth showed that Li tends to be close to the bridging nitrogen in phosphorus oxynitrides compared to BO in phosphorus oxides [35] [43]. This suggests that bridging nitrogen

has a stronger influence on the Li environment than BO, and gives rise to a non-negligible ionic interaction between Li ions and the bridging nitrogen. Thus, nitrogen atoms could be linked to two phosphorus atoms with covalent bonds and one Li ion with a weak ionic bond, as shown in Figure S6 of Supporting Information. The stronger involvement of bridging nitrogen atoms in the bound sphere of Li ions leads to a more uniform distribution of negative charge density along chain structures with a -P-N-P-N- backbone, compared to phosphorus oxide networks where the negative charge is located mainly at NBO sites [31]. Such charge delocalization along the phospho-nitride chains may contribute to the increased Li ion transport. Further research is needed to clarify the orign of high ionic conductivity in ALD LiPON films.

4. Conclusions

In this study, new plasma-assisted ALD processes were successfully developed in order to deposit lithium phosphate and LiPON SSE thin films using LiO^{t}Bu and TDMAP precursors with H_2O oxidant and different plasma reactants, in the deposition temperature range of between 220 and 300 °C. The films deposited with O_2 plasma produced a polycrystalline lithium phosphate with a relatively well-arranged pyrophosphate, while the films deposited with Ar and NH_3 plasma produced an amorphous LiPON with a mixture of pyrophosphate and orthophosphate. The elemental composition varied from $Li_{3.3}PO_{3.4}$ for O_2 plasma to $Li_{2.8}PO_{2.9}N_{0.2}$ for Ar plasma and $Li_{2.5}LiPO_{1.9}N_{0.8}$ for NH_3 plasma with a 20 sccm flow rate. With increased NH_3 flow rate, the nitrogen composition increased up to ~13% while keeping residual carbon to below a few percent. The lithium phosphate films deposited with O_2 plasma exhibited an ionic conductivity of $1.75 \pm 0.52 \times 10^{-9}$ S cm^{-1} at 25 °C, with an activation energy of 0.9 eV. On the other hand, the ionic conductivity of LiPON films deposited with NH_3 plasma increased to $1.65 \pm 0.42 \times 10^{-6}$ S/cm, with an activation energy of 0.66 eV. This conductivity is the highest value for any ALD LiPON film reported to date. Finally, an ALD growth mechanism was proposed for different plasma reactants. Our ALD processes demonstrate the good controllability of the molecular structures of the phosphate matrices with high ionic conductivity for realizing high-performance Li-based SSE thin films, which can be used not only for microbatteries but also for neuromorphic devices.

ASSOCIATED CONTENT

Supporting Information

The Supporting Information is available free of charge on the ACS Publication website at DOI:
Growth-rate versus pulse-time of H_2O and TDMAP, FTIR spectra of LiPON films deposited at 300 and 220 °C with NH_3 plasma of 20 sccm flow rate, high-resolution core-level spectra of P 2p

and Li 1s, elemental composition of films deposited at 220 °C, Arrhenius plots of the ionic conductivity of films deposited at 300 and 220 °C with O_2 and Ar plasma, an XRR curve with fitting curves calculated based on a multi-layer model, evaluated for a LiPON film deposited with Ar plasma, and another possible growth mechanism for ALD lithium phosphate and LiPON films.

AUTHOR INFORMATION

Corresponding author

*E-mail: TSURUOKA.Tohru@nims.go.jp

Notes

The authors declare no competing financial interests.

ACKNOWLEDGMENTS

We would like to thank H. Yasufuku and S. Sueya for their assistance with the HAXPES and XRR measurements and S. Yasuhara (Japan Advanced Chemicals Ltd.) for a fruitful discussion on the growth mechanism. This work was in part supported by the Panasonic-NIMS Center of Excellence for Advanced Functional Materials, JSPS KAKENHI Grant Number 21H03412, and 'Advanced Research Infrastructure for Materials and Nanotechnology in Japan (ARIM)' of the Ministry of Education, Culture, Sports, Science and Technology (MEXT). Proposal Number JPMXP1223NM5065.

REFERENCES

[1] Bruce, P. G.; Scrosati, B.; Tarascon, J. M. Nanomaterials for rechargeable lithium batteries. Angw. Chem. Int. Ed. **2008**, 47, 2930-2946.

[2] Palacín, M. R.; de Guibert, A. Why do batteris fail? Science. **2016**, 351 (6273) 574-582.

[3] Ping, W.; Yang C.; Bao, Y.; Wang, C.; Xie, H.; Hitz E.; Cheng, J.; Li, T.; Hu, L. A silicon anode for garnet-based all-solid-state batteries: Interfaces and nanomechanics. Energy Storage Mater. **2019**, 21, 246-252.

[4] Deng, J.; Bae, C.; Denlinger, A.; Miller, T. Electric vehicles batteries: Requirements and Challenges. Joule. **2020**, 4, 511-515.

[5] Sood, A.; Poletayev, A. D.; Cogswell, D. A.; Csernica, P. M.; Mefford, J. T.; Fraggedakis, D.; Toney, M. F.; Lindenberg, A. M.; Bazant, M. Z.; Chueh, W. C. Electrochemical ion insertion from the atomic to the device scale. Nature Rev. Mater. **2021**, 6, 847-867.

[6] Fuller, E. J.; Gabaly, F. E.; Léonard, F.; Agarwal, S.; Plimpton, S. J.; Jacobs-Gedrim, R. B.; James, C. D.; Marinella, M. J.; Talin, A. A. Li-ion synaptic transistor for low power analog computing. Adv. Mater. **2017**, 29, 1604310.

[7] Nikam, R. D.; Kwak, M.; Lee, J.; Rajput, K. G.; Banerjee, W.; Hwang, H. Near ideal synaptic functionalities in Li ion synaptic transistor using $Li_3PO_xSe_x$ electrolyte with high ionic conductivity. Sci. Rep., **2019**, 9, 18883.

[8] Wan, X.; Tsuruoka, T.; Terabe, K. Neuromorphic system for edge information encoding: Emulating retinal center-surround antagonism by Li-ion-mediated highly interactive devices. Nano Lett. **2021**, 21, 7938-7945.

[9] Marukame, T.; Mizushima, K.; Nomura, K.; Nishi, Y. Lithium-ion-based resistive devices of $LiCoO_2$/LiPON/Cu with ultrathin interlayers of titanium oxide for neuromorphic computing. *IEEE J. Electron Devices Soc.* **2023**, 11, 602-610.

[10] Mallik, S.; Tsuruoka, T.; Tsuchiya, T.; Terabe, K. Effects of Mg doping to a $LiCoO_2$ channel on the synaptic plasticity of Li ion-gated transistors. ACS Appl. Mater. Interfaces. 2023, 15, 47184-47195.

[11] Yu, X.; Bates, J. B.; Jellison, G. E.; Hart, F. X.; A stable thin-film lithium electrolyte: lithium phosphorus oxynitride. J. Electrochem. Soc. **1997**, 144, 524-531.

[12] Zhao, S.; Fu, Z.; Qin, Q. A solid-state electrolyte lithium phosphorus oxynitride film prepared by pulsed laser deposition. Thin Soild Films. **2002**, 415, 108-113.

[13] Kim, H. T.; Mun, T.; Park, C.; Jin, S. W.; Park, H. Y. Characteristics of lithium phosphorous oxynitride thin films deposited by metal-organic chemical vapor deposition technique. J. Power Souces. **2021**, 244, 641-645.

[14] Han, L.; Hsieh, C. -T.; Mallick, B. C.; Li, J.; Gandomi, Y. A. Recent progress and future prospects of atomic layer deposition to prepare/modify solid-state electrolytes and interfaces between electrodes for next-generation lithium batteries. Nanocale Adv. **2021**, 3, 2728-2740.

[15] Kozen, A. C.; Pearse, A. J.; Lin, C. -F.; Noked, M.; Rubloff, G. W. Atomic layer deposition of the solid electrolyte LiPON. Chem. Mater. **2015**, 27, 5324-5331.

[16] Nisula, M.; Shindo, Y.; Koga, H. Karppinen, M. Atomic layer deposition of lithium phosphorus oxynitride. Chem. Mater. **2015**, 27, 6987-6993.

[17] Pearse, A.; Schmitt, T. E.; Fuller, E. J.; El-Gabaly, F.; Lin, C. -F.; Gerasopoulos, K.; Kozen, A. C.; Talin, A. A.; Rubloff, G.; Gregorczyk, K. E. Nanoscale solid state batteries enabled by thermal atomic layer deposition of a lithium polyphosphazene solid state electrolyte. Chem. Mater. **2017**, 29, 3740-3753.

[18] Put, B. Mees, M. J.; Hornsveld, N.; Hollevoet, S.; Sepúlveda, A.; Vereecken, P. M.; Kessels, W. M. M.; Creatore, M. Plasma-assisted ALD of LiPO(N) for solid state batteries. J. Electrochem. Soc. **2019**, 166, A1239-A1242.

[19] Su, J.; Tsuruoka, T.; Tsujita, T.; Nishitani, Y.; Nakura, K.; Terabe, K. Atomic layer deposition of a mangesium phosphate solid electrolyte. Chem. Mater. **2019**, 31, 5566-5575.

[20] Tsuruoka, T.; Tsujita, T.; Su, J.; Nishitani, Y.; Hamanura, T.; Inatomi, Y.; Nakura, K.; Terabe, K. Fabrication of a magnesium-ion-conducting magnesium phosphate electrolyte film using

atomic layer deposition. Jpn. J. Appl. Phys. **2020**, 59, SIIG08.

[21] Su, J.; Tsuruoka, T.; Tsujita, T.; Inatomi, Y.; Terabe, K. Nitrogen plasma enhanced low temperature atomic layer deposition of magnesium phosphorus oxynitride (MgPON) solid-state electrolyte. Angew. Chem. Int. Ed. **2023**, 62, e202217203.

[22] Shibata, S. Thermal atomic layer deposition of lithium phosphorus oxynitride as a thin-film electrolyte. J. Electrochem. Soc. **2016**, 163, A2555-A2562.

[23] Wang, B.; Liu, J.; Li, R.; Sham, T. -K.; Sun, X. Atomic layer deposition of lithium phosphates as solid-sate electrolytes for all-solid-state microbatteries. Nanotechnology. **2014**, 25, 504007.

[24] Hämäläinen, J.; Holopainen, J.; Munnik, F.; Hatanpää, T.; Heikkilü, M.; Ritala, M.; Leskelä, M. Lithium phosphate thin films grown by atomic layer deposition. J. Electrochem. Soc. **2021**, 159, A259-A263.

[25] Ayu, N. I. P.; Kartini, E.; Prayogi, L. D.; Faisal, M. Crystal structure analysis of Li_3PO_4 powder prepared by wet chemical reaction and solid-state reaction by using X-ray diffraction (XRD). Ionics. **2016**, 22, 1051-1057.

[26] Fantin, R.; Van Roekeghem, A.; Benayad, A. Revisiting Co 2p core-level photoemission in $LiCoO_2$ by in-lab soft and hard X-ray photoelectron spectroscopy: A depth-dependent study of cobalt electronic structure. Surf. Interface Anal. **2022**, 55, 489-495.

[27] Jacke, S.; Song, J.; Cherkashinim, G.; Dimesso, L.; Jaegermann, W. Investigation of the solid-state electrolyte/cathode LiPON/$LiCoO_2$ interface by photoelectron spectroscopy. Ionics. **2010**, 16, 769-775.

[28] Fleutot, B.; Pecquenard, B.; Martinez, H.; Levasseur, A. Thorough study of the local structure of LiPON thin films to better understand the influence of a solder-reflow type thermal treatment on their performances. Solid State Ionics. **2012**, 206, 72-77.

[29] Mani, P. D.; Saraf, S.; Sinh, V.; Real-Robert, M.; Vijayakumar, A.; Dueanceau, S. J.; Seal, S.; Coffey, K. R. Ionic conductivity of bias sputtered lithium phosphorus oxy-nitride thin films. Solid State Ionics. **2016**, 287, 48-59.

[30] Kamitsos, E. I.; Dussauze, M.; Varsamis, C. -P. E.; Vinatier, P.; Hamon, Y. Thin film amorphous electrolytes: structure and composition by experimental and simulated infrared spectra. J. Phys. Chem. C. **2007**, 111, 8111-8119.

[31] Carrillo Solano, M. A.; Dussauze, M.; Vinatier, P.; Croguennec, L.; Kamitsos, E. I.; Hausbrand, R.; Jaegermann, W. Phosphate structure and Lithium environments in lithium phosphorus oxynitride amorphous thin films. Ionics. **2016**, 22, 471-481.

[32] Corbridge, D. E. C.; Lowe, E. J. The infra-red spectra of some inorganic phosphorus compounds. J. Chem. Soc. **1954**, 493-502.

[33] Veli, L. L.; Varsamis, C. -P. E.; Kamitsos, E. I.; Möncke, D.; Ehrt, D. Structural investigation of metaphosphate glasses. Phys. Chem. Glasses. **2005**, 46, 178-181.

[34] Cai, W.; Chen, R.; Yang, Y.; Yi, M.; Xiang, L. Removal of SO_4^{2-} from Li_2CO_3 by recrystallization in Na_2CO_3 solution. Crystals. **2018**, 8, 19.

[35] Du, Y. A.; Holzwarth, N. A. W. First-principle study of LiPON and related solid electrolyes. Rhys. Rev. B. **2010**, 81, 184106.

[36] Tsuruoka, T.; Su, J.; Terabe, K. A voltage-controlled oscillator using variable capacitors with a thin dielectric electrolyte film. ACS Appl. Electron. Mater. **2020**, 2, 2788-2797.

[37] Meyer, K.; Hobert, H.; Barz, A.; Stachel, D. Infrared spectra and structure of various crystalline ultraphosphates and their glasses. Vib. Spectrosc. **1994**, 6, 323-332.

[38] Hoppe, U. A structural model for phosphate glasses. J. Non-Cryst. Solids. **1996**, 195, 138-147.

[39] Hoppe, U.; Walter, G.; Barz, A.; Stachel, D.; Hannon, A. C. The P-O bond lengths in vitreous probed by neutron diffraction with high real-space resolution. J. Phys.: Condens. Matter. **1998**, 10, 261-270.

[40] Brow, R. K. The structure of simple phosphate glasses. J. Non-Cryst. Solids. **2000**, 263-264, 1-28.

[41] Chatterjee, A.; Ghosh, A. Correlation between ion transport and network structure of Li_2O-P_2O_5 glasses. Solid State Ionics. **2018**, 314, 1-8.

[42] Kazyak, E.; Chen, K. -H.; Davis, A. L.; Yu, S.; Sanchez, A. J.; Lasso, J.; Bielinski, A. R.; Thompson,T.; Sakamoto, J.; Siegel, D. J.; Dasgupta, N. P. Atomic layer deposition and first principles modeling of glassy Li_3BO_3-Li_2CO_3 electrolytes for solid-state Li metal batteries. J. Mater. Chem. A. **2018**, 6, 19425-19437.

[43] Du, Y. A.; Holzwarth N. A. W. Effects of O vacancies and N or Si substitutions on Li^+ migration in Li_3PO_4 electrolytes from first principles. Phys. Rev. B, **2008**, 78, 174301.

For Table of Contents Only